2022 SCEC Report

Project #22056

Informing Rupture Directivity Modeling with CyberShake Simulations

Jeff Bayless and Norman Abrahamson

AECOM, Los Angeles

August 4, 2023

Thanks to SCEC for funding this work under Award #22056, to Xiaofeng Meng for sharing CyberShake residuals, and to Kevin Milner and Scott Callaghan for answering CyberShake-related questions.

Table of Contents

Abstract

In this study, a database of near-fault CyberShake simulations, consisting of many earthquake sources with multiple hypocenters and rupture realizations, is used to evaluate rupture directivity effects in the simulated ground motions. CyberShake ground motion residuals are calculated from the Meng et al. (2023; Mea23) ground motion model (GMM) to explicitly quantify the directivity effects. The Mea23 model is created from the CyberShake simulations, and their residual analysis includes careful treatment of source, path, and site effects. The residuals are used to qualitatively evaluate the Bayless et al. (2020; Bea20) median directivity model. Then, the CyberShake scenario earthquakes and their multiple hypocenter realizations are used to improve one component of the Bea20 model that has remained unresolved due to lack of available recorded data: the appropriate aleatory variability adjustment.

The overall performance of Bea20 as compared with the simulation residuals is promising, but wide-ranging. There are many instances of source and hypocenter location with residuals matching Bea20 quite well, and there are many instances which do not match as well. This is the same observation Bea20 made with respect to the recorded data used to develop their model. Peak amplitudes of mean simulation residuals are found to be generally lower than the mean Bea20 predictions, and the variance of the simulation residuals are found to be generally larger than Bea20. Nonetheless, modeling improvements gained by incorporating Bea20 are quantified through residual variance reductions. At T=5 sec, residual variance reductions of between 0.05 and 0.09 are found. This reduction is larger than the empirically derived reduction from Bea20, which is based on a relatively sparse dataset, and represents about a 12% reduction in one component of the aleatory variability, which is large enough to be impactful in seismic hazard applications.

1. Introduction

Over the past decade-plus, the Broadband Platform (Goulet et al., 2015) and SCEC CyberShake research projects (Graves et al. 2011) have made tremendous progress in ground motion simulations. CyberShake is a computational study to calculate ground motion hazard in the Los Angeles region (Graves et al., 2011, and subsequent updates). Others have used CyberShake for ground motion studies and simulation validation, e.g. Chen and Baker (2019); Wang and Jordan (2014); Villani and Abrahamson (2015); and our 2020 SCEC project (Award #20043). CyberShake v15.4 includes simulations of over 415,000 UCERF2 rupture realizations at 336 sites, and simulates wave propagation through a three-dimensional velocity model that reflects the impact of sedimentary basins and near-surface materials on ground motion (Chen and Baker, 2019).

These wave-propagation simulations are well suited to quantify rupture directivity effects on the resulting ground motions. However, the explicit separation and quantification of rupture directivity effects in CyberShake ground motions has not been well-studied. In Bayless et al. (2020; Bea20 hereafter), we developed a rupture directivity ground motion adjustment model based on NGA-West2 (Bozorgnia et al., 2014) data and on an ensemble of simulations, including those performed on the SCEC Broadband Platform and by others for 1D velocity structure, but not including CyberShake.

In this study, a database of near-fault CyberShake simulations, consisting of earthquake sources with multiple hypocenters and rupture realizations and both 1D and 3D velocity models, is used to evaluate rupture directivity effects in the simulated ground motions. CyberShake ground motion residuals are calculated from the Meng et al. (2023; Mea23) ground motion model (GMM) to explicitly quantify the directivity effects. The Mea23 model is created from the CyberShake simulations, and the residual analysis includes careful treatment of source, path, and site effects.

The residuals are used to evaluate the Bayless et al. (2020; Bea20) median directivity model. Then, the CyberShake scenario earthquakes and their multiple hypocenter realizations are used to improve one component of the Bea20 model that has remained unresolved due to lack of available recorded data: the appropriate aleatory variability adjustment.

2. Background

It is well known that ground motions under forward directivity conditions have amplified intensity (Somerville et al., 1997). Forward directivigy ismore likely at a site locates near the ends of the rupture and thus can increase the seismic hazard at a site located at the end of a fault relative to a site located near the center of the fault which is more likey to experience backward directivity (e.g. Abrahamson, 2000; Shahi, 2013; Tarbali et al., 2016, Spagnulo et al., 2012). This effect, along with the effect on the seismic hazard deaggregation, is illustrated in Figure 1 (from Tarbali et al., 2016) for an example site in Los Angeles. Methods to include directivity effects in probabilistic seismic hazard assessments (PSHAs) have been proposed in the literature (e.g., Abrahamson, 2000; Tothong et al., 2007; Shahi, 2013; Rodriguez-Marek and Cofer, 2009, Donahue et al., 2019, Watson-Lamprey, 2018). In the response spectral approach, which we adopt, rupture directivity effects are incorporated by modifications to the elastic acceleration response spectrum at 5% damping. This approach lends itself readily to inclusion into PSHA (Rodriguez-Marek and Cofer, 2009).

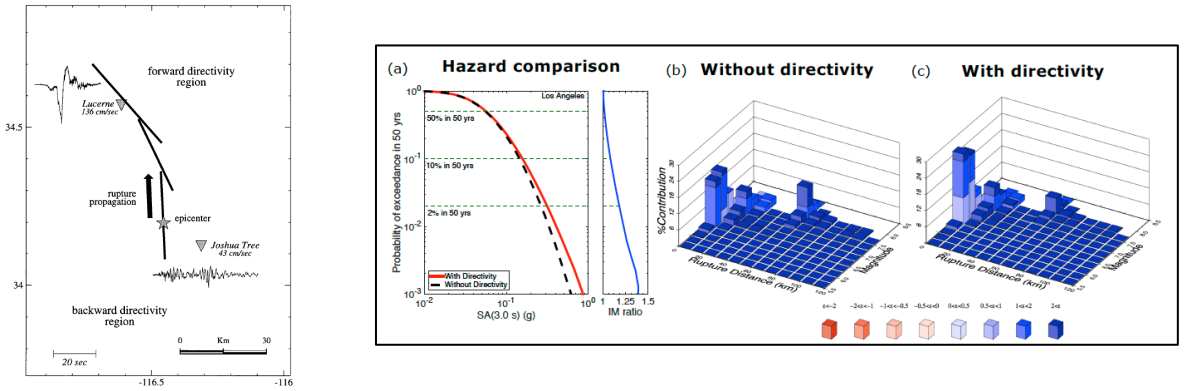

Figure 1. Left: Map of the 1992 Landers earthquake region, including velocity waveforms at the Lucerne (forward directivity) and Joshua Tree sites. Source: Somerville et al., 1997. Right: (a) Sa at T=3.0s hazard curves and (b)-(c) deaggregation results for Los Angeles at 2% in 50 years exceedance probability, with and without considering directivity effects using the Shahi and Baker (2013) pulse model. Source: Tarbali (2016)

The effects of rupture directivity on near-fault ground motions are known to be significant and should be included to accurately estimate the hazard from long period ground motions (Abrahamson, 2000). However, these effects are not explicitly accounted for in typical GMMs, and therefore not in typical PSHAs. The obstacles preventing typical PSHAs from including directivity effects are:

1. The added computational complexity required to include them, derived from the need to model random variations in hypocenter location.
2. Uncertainty in practice about which directivity model or models to use, how to use them, and how to calculate the required directivity parameters.
3. The compatibility of the directivity model with the median GMM may not be clear (what is the average directivity condition in the empirival data used to develop the GMM?)
4. The appropriate reduction in the aleatory variability has not been determined.

As described by Abrahamson (2000) in relation to the first obstacle, sampling the hypocenter locations from a distribution to account for rupture directivity effects adds substantial computational costs to the hazard calculation, so this is not always performed. However, for most modern hazard analysts, large computation costs are manageable and so this obstacle is readily overcome. In Bea20, we addressed the uncertainties of the second obstacle. The average directivity condition implicit in the GMMs was evaluated by Donahue et al. (2019), leaving the fourth obstacle to be addressed.

In this study, we validate the explicit rupture directivity effects on ground motions in the CyberShake simulations by comparing them with the empirical model and address the fourth obstacle from the list above.

Additional Background on the Aleatory Variability

There are two components of aleatory variability associated with adding a directivity model in PSHA. One is the reduction of the GMM variability due to improvements in the median prediction – this is the reduction in variability caused by including the directivity term in GMM regression. The second component is the added aleatory variability due to randomizing the location of the hypocetner for future earthquakes (each with a different directivity adjustment). Watson-Lamprey (2018) used the following notation for these components:

$$\sigma_i^2 = \sigma_{GMM}^2 - \sigma_{Reduction}^2 + \sigma_{i|RH}^2 \quad (1)$$

where σ_i is the total aleatory variability at site i, σ_{GMM} is the published GMM aleatory variability (no directivity), $\sigma_{Reduction}$ is the reduction in variability by improving the fit to the observation due to including the directivity parameter in the GMM, and $\sigma_{i|RH}$ is the aleatory variability of the change in the median at a given site due to including directivity effects in the GMM from all sources and hypocenters (here RH stands for random hypocenters). The $\sigma_{Reduction}$ and $\sigma_{i|RH}$ are specific to a directivity model.

Watson-Lamprey (2018) created models for estimating the total aleatory variability, σ_i, using the directivity predictor DPP (Spudich et al., 2013) in the absence of any other recommendations in the literature. These models can be used to account for the effects of directivity in PSHA without modeling the variability of the hypocenter location in the hazard calculation. Therefore, in Watson-Lamprey (2018) and in Equation 1 above, the $\sigma_{i|RH}^2$ term is explicitly added to the total variability.

However, if hypocenter locations are modeled (e.g. PSHA Option 5 from Donahue et al., 2019) then this standard deviation is implicitly accounted for within the PSHA integral, and the aleatory variability to use with a GMM-directivity model pair is:

$$\sigma_{i,PSHA}^2 = \sigma_{GMM}^2 - \sigma_{Reduction}^2 \quad (2)$$

In the case of Equation 2, an average $\sigma_{i|RH}$ is not evaluated directly, but rather a site-specific non-parametric variability is included through the hazard integral over the hypocenter location.

If $\sigma_{i|RH}$ is larger than $\sigma_{Reduction}$, the net standard deviation adjustment is positive, implying that the variability from directivity for a random site is larger than the range of expected directivity effects from the distribution of stations in the data set. Alternatively, a net negative adjustment implies the opposite. Either assumption requires justification and neither has been documented in the literature; this is the main cause of confusion in practice about how to treat directivity effects in PSHA (Donahue et al., 2019). In this study the simulations are used to gain insight into the appropriate values for $\sigma_{Reduction}$ with the Bea20 model.

3. CyberShake Simulations

Meng et al. (2023) compared the CyberShake platform simulations against the Next Generation Attenuation-West2 empirical datasets. Because the CyberShake and empirical datasets cover very different magnitude ranges and site conditions, Mea23 developed GMMs from the CyberShake simulations for this purpose. Four CyberShake simulation datasets were evaluated by Mea23: CS15.4 in southern California, CS17.3 (1D and 3D versions) in central California, and CS18.8 in northern California. The Mea23 GMMs are for the RotD50 component of spectral acceleration at periods 2, 3, 5, and 10 sec and do not have components for directivity effects. The residuals are decomposed following Villani and Abrahamson (2015) into event terms, site terms, path terms, and remaining residuals. The notation for the remaining residual in natural log units is δW_0.

The CS17.3 simulations for central California are selected for this study. CS17.3 has 1D and 3D versions, which means the simulations of the same set of scenarios are performed using a plane-layered (1D) seismic velocity model, and using a 3D seismic velocity model; each velocity model has its own associated simulation method. Because both versions are available, the impact of the differences in these methodologies on rupture directivity can be readily investigated. Additionally, out of the three CyberShake study regions, the central CA region is expected to have the weakest basin effects. Bea20 found that basin effects can interfere with rupture directivity studies based on residuals, because of their long period nature and their spatial correlation, therefore it is preferable to avoid basins to the extent possible.

The CS17.3 sources are based on the UCERF2 model (Field et al., 2009). For this study, all the events with rupture extent completely within the footprint of the 438 sites are selected (Figure 1). This results in 1667 ruptures on 45 named faults. Each of these ruptures has multiple hypocenter location realizations, ranging from several dozens to several hundred of realizations depending on the rupture dimensions (Figure 2). The resulting dataset is over 33 million simulated ground motion time histories, from which the response spectra are calculated.

The distributions of source parameters moment magnitude, average rake, and fault dip are shown in Figure 2. Out of this subset, 1034 ruptures are categorized as strike-slip based on average rake angle (absolute value of average rake less than 60 degrees or greater than 120 degrees). The remainder of this study focuses on these strike-slip scenarios and their simulations.

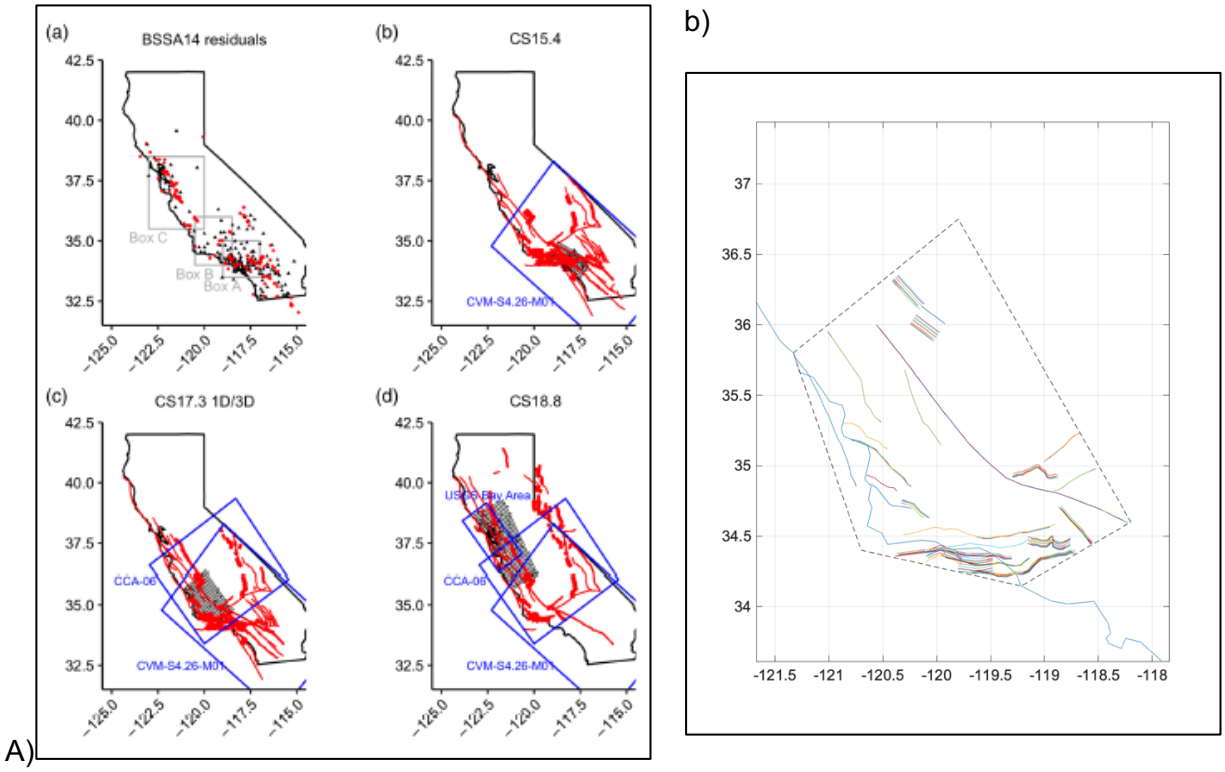

Figure 1. (a) Maps of the CyberShake stations and hypocenters by CyberShake study, from Meng et al. (2023). (b) A map of the CS17.3 fault traces from the set of selected simulations for this study.

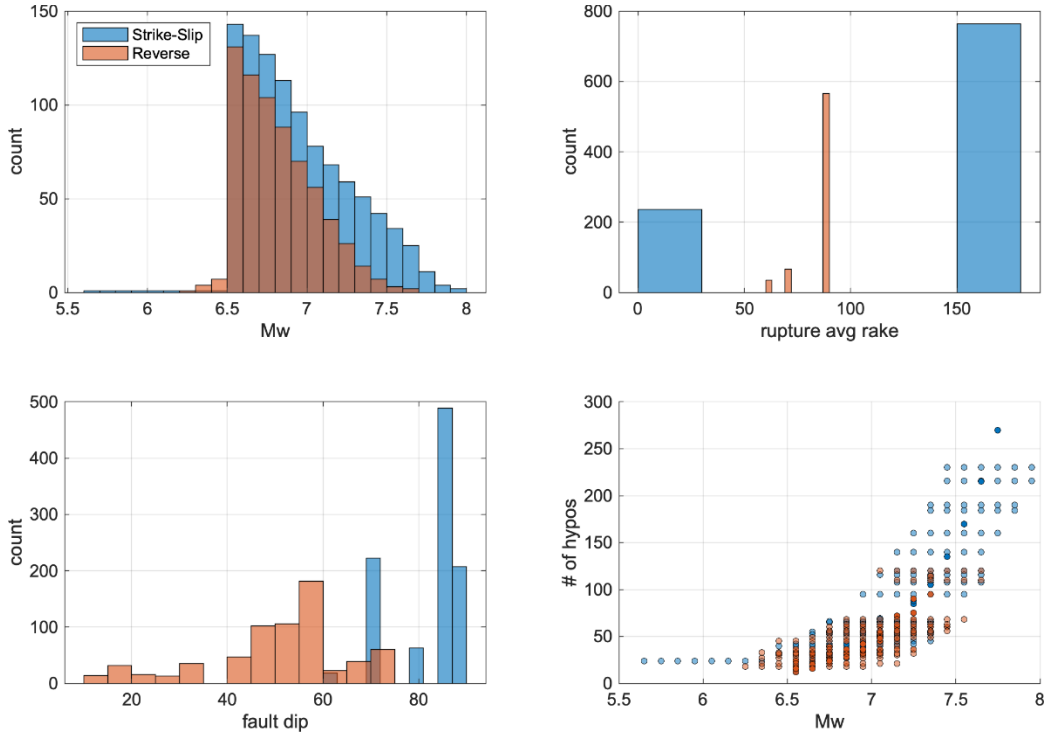

Figure 2. Distributions of source parameters of the selected CS17.3 simulations, and the count of hypocenter variations with moment magnitude.

Although directivity effects were not the focus of their study, Mea23 quantified the directivity effects in CyberShake by computing the average directivity effects from each event to all sites for CyberShake datasets following the Spudich et al. (2013) model. They found that the majority of events had average directivity effects close to zero and that only events initiated near the two ends of the San Andreas fault have positive directivity effects up to 0.2 in natural log units, concluding that directivity does contribute to large ground motions for some events, but its effects are largely negligible considering the whole dataset. Mea23 also compared residual maps between the 1D and 3D simulations and found quite similar patterns, nothing that the radiation pattern and Moho bounce signals are much stronger in 1D simulations (Xiaofeng Meng, personal communication).

4. Rupture Directivity Analysis

4.1 Procedure

Using the database described above, the Mea23 GMM is used to calculate the RotD50-component δW_0 at spectral periods 2, 3, 5, and 10 sec. The δW_0 residuals are the remaining residuals after accounting for the median GMM plus any repeatable source, path, and site effects. In this study, δW_0 are used as a proxy to represent rupture directivity effects, acknowledging that the δW_0 represent the total 'remaining' or 'unmodeled' ground motion features, including rupture directivity effects in addition to any other unexplained or unmodeled features of the ground motions.

For each earthquake scenario and for each hypocenter realization of that scenario, the Bea20 model is used to calculate the predicted directivity adjustment in natural log units (f_D) at all simulation stations. The f_D is a 'centered' version of Bea20 in which all sites with a given rupture distance have a mean directivity adjustment equal to zero. The centering ensures that the magnitude and distance scaling of the GMM is not altered by incorporating the directivity adjustment. This also assumes that the data used in the GMM reflects average directivity conditions for uniformly distributed sites. (i.e., the GMM is unbiased in terms of directivity effects).

The residuals δW_0 are adjusted for directivity by removing the centered f_D. The quantity [$\delta W_0 - f_D$] is denoted δW_{0Dir}; this represents the remaining residual after accounting for rupture directivity. The standard deviations of δW_0 and δW_{0Dir} are ϕ_0 and ϕ_{0Dir}, respectively.

This process is repeated for all hypocenter realizations of a given scenario. The multiple hypocenter realizations are used to calculate standard deviations at a given site; this is the variability at a given site from rupture directivity due to differences in hypocenter location.

Additionally, the residuals from multiple hypocenter realizations are treated as distinct scenarios and pooled together to estimate the total standard deviation reductions which result from including the Bea20 model. The latter can be used to estimate $\sigma^2_{Reduction}$ from Eqs. 1 and 2, where the symbol σ, for the total standard deviation, is replaced with ϕ, for the standard deviation of the remaining residual after adjusting for source, path, site, and directivity effects.

4.2 Results: Individual Scenarios

Individual scenario (defined as one earthquake and hypocenter realization) evaluations are used as a qualitative test of the Bea20 performance for median directivity. Each evaluation is performed for the same scenarios using the 1D and 3D simulation results. A subset of earthquake scenarios, randomly selected from the larger set of 1034, are evaluated as follows.

The scenario used as an example is a vertically dipping strike-slip rupture on a section of the San Andreas fault, with Mw 7.15 and Ztor=0 km (depth to the top of the rupture plane), using the 1D simulation. Figure 3 compares maps of δW_0, f_D, and δW_{0Dir} (T=5 sec) for one hypocenter

realization of this scenario earthquake. Triangles in Figure 3 are the CS17.3 simulation stations, the solid black line represents the fault trace, and the red star represents the hypocenter location, which is located at approximately mid-depth in this example.

Figure 3 shows that, for this scenario and hypocenter realization, the δW_0 residuals are generally positive (representing higher than average ground motions for a given distance) off the ends of the rupture plane and are generally negative (lower than average ground motions) between the ends of the rupture plane. Both are expected features for a large magnitude vertical strike-slip earthquake and are present to some degree in the Bea20 model predictions (f_D, top right of Figure 3). The map of f_D also has an amplification pattern reflecting the SH radiation pattern lobes for a strike-slip point-source double couple at the hypocenter; this is visible as a faint blue 'X' pattern centered on the hypocenter.

The remaining residuals after removing the directivity prediction (δW_{0Dir}) are shown in the bottom left panel of Figure 3. Examining this example map by eye, the δW_{0Dir} appear to have an improved fit to the simulation data, with less "hot" and "cold" areas on average than δW_0. This is especially apparent off the ends of the fault plane (forward directivity zones in a strike-slip earthquake). An improved fit to the simulation residuals will correspond to a reduction in aleatory variability.

Figure 3 also shows the δW_0 and δW_{0Dir} versus rupture distance, with their standard deviations (for all distances): ϕ_0 and ϕ_{0Dir}. The reduction in aleatory variability is represented as a difference in variances:

$$\phi^2_{Reduction} = \phi^2_0 - \phi^2_{0Dir} \quad (3)$$

In this example, the variance reduction, $\phi^2_{Reduction}$, is approximately 0.072.

The analysis shown in Figure 3 is repeated for all the 108 hypocenter realizations of this scenario; the results considering the multiple hypocenter realizations are covered in Section 4.3.

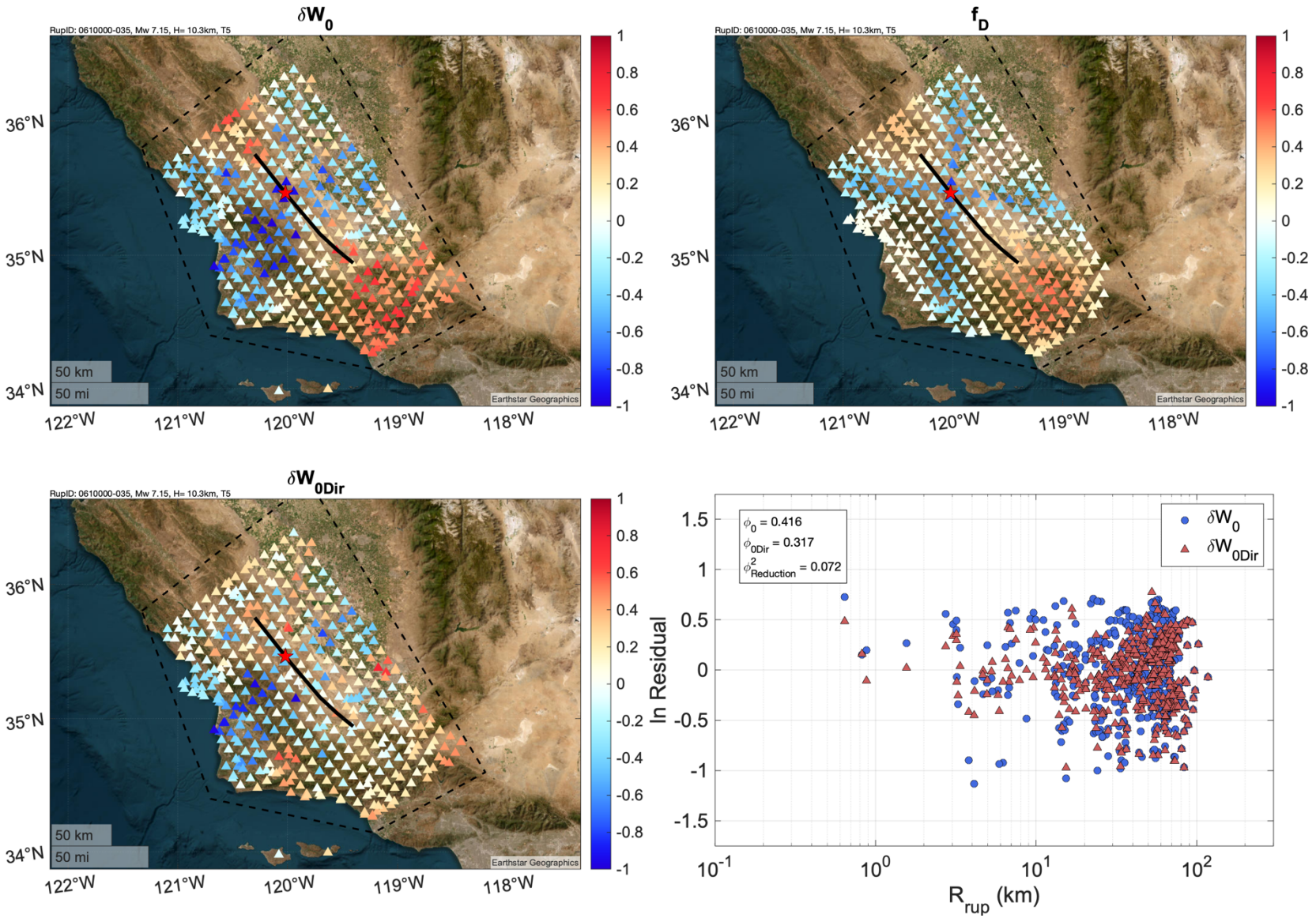

Figure 3. Results for one hypocenter realization of an example San Andreas scenario earthquake. Maps are of δW_0, f_D, and δW_{0Dir} (T=5 sec). At bottom right, residuals versus distance before and after adjusting for directivity.

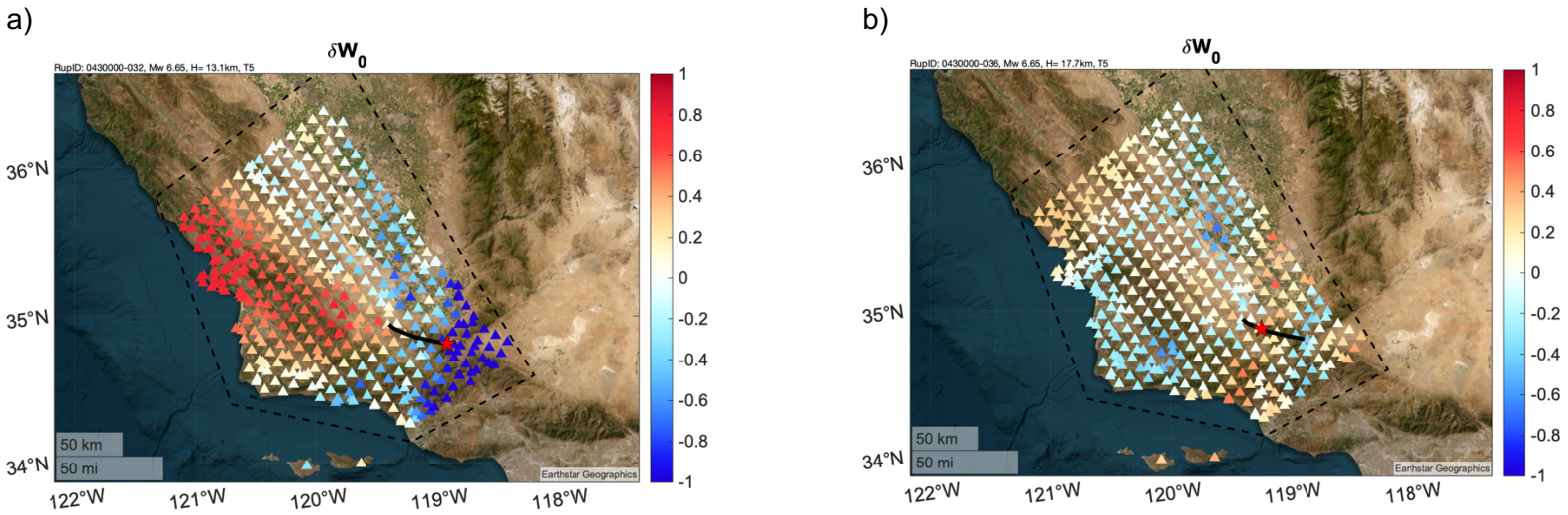

Figure 4. Maps of CS17.3 δW_0 at T=5 sec for a Mw 6.65 scenario earthquake with two different hypocenters showing (a) very large amplitude residuals with strong azimuthal variation and (b) smaller amplitude residuals with weaker azimuthal variation.

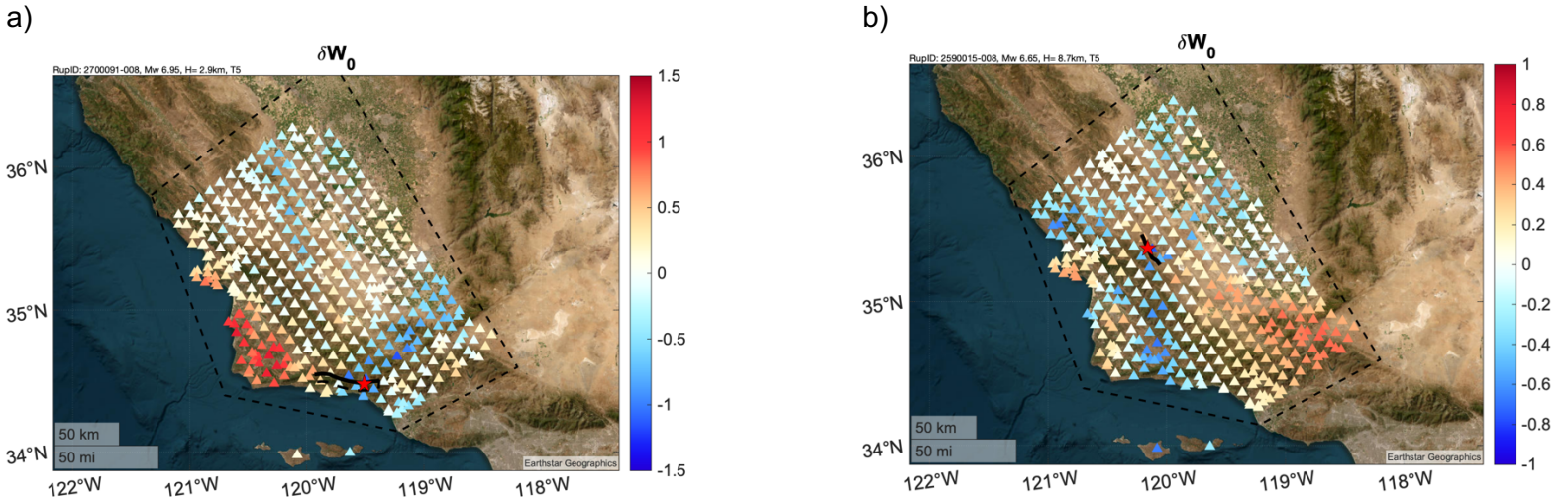

Figure 5. Maps of CS17.3 δW_0 at T=5 sec. (a) a Mw 6.95 scenario earthquake with residual patterns broadly compatible with Bea20 and (b) a Mw 6.65 scenario earthquake with unexpected residual patterns.

Discussion

The simplest evaluation method of Bea20 is a subjective comparison of the CS17.3 simulation residuals (δW_0) with f_D. As a first step, this requires assessment of the δW_0. Overall, the δW_0 exhibit a wide range of apparent rupture directivity effects. In some instances of earthquake scenario and hypocenter location, the δW_0 have quite large amplitudes (absolute values greater than 1.5 natural log units) and systematic variations with azimuth. In other similar hypocenter realizations, δW_0 amplitudes are much smaller and with limited azimuthal variation. Figure 4 shows two such examples from one scenario earthquake with Mw 6.55.

This inconsistent behavior of the δW_0 is hypothesized to be related to the earthquake source, determined in part by process of elimination. The behavior is observed in both the 1D and 3D simulations, implying that the differences are not due to differences in path models. The CS17.3 near-surface site conditions have limited resolution and variability, so local site effects should be relatively minor, in particular between different realizations of the same earthquake. The remaining component of the simulations is the earthquake source. The simulations use kinematic models of finite-fault ruptures, or 'slip models' for short, to describe the spatial and temporal heterogeneity in the slip function. CS17.3 uses the Graves and Pitarka (2014) method for generating the slip model of each scenario earthquake. Graves and Pitarka (2016) introduced fault roughness and velocity perturbation features, which act to reduce the coherence of the radiated motions mostly at high frequencies, into a revised methodology for generating kinematic earthquake rupture models. This method was not available at the time of the CS17.3 simulations.

The two conditions for forward rupture directivity given by Somerville et al. (1997) are rupture front propagation toward the site and slip in the same direction as the rupture propagation. Bea20 assumes that the earthquake rupture is, to some degree, propagating in the same direction as the slip. In reality, the direction of rupture propagation and its consistency with the slip direction will affect the degree of rupture directivity (Aagaard et al., 2004). The inconsistencies observed in residual patterns and amplitudes between similar earthquake realizations (e.g., Figure 4) may reflect the complexities of this phenomenon as contained in the CS17.3 slip models; the directivity in the simulated ground motions for a given earthquake scenario and hypocenter location will depend on the coherency of slip, slip direction, and rupture direction in the slip model.

Another assumption in Bea20 is that rupture is bilateral, travels approximately parallel to the ground surface in both directions, and travels from some depth upward towards the ground surface. In the strike-slip case, the bilateral assumption of the rupture means that forward directivity effects are modeled, to some degree, at either end of the rupture from the hypocenter. This has the potential to over-estimate the ground motion amplification due to directivity in the case of a unilateral ruptures in the CS17.3 slip models.

Because of these reasons, the overall performance of Bea20 as compared with the CS17.3 δW_0 is promising, but wide-ranging. There are many instances of source and hypocenter location with residuals matching Bea20 quite well (e.g. Figure 3), and there are many instances which do not match well. This is the same observation Bea20 made with respect to the recorded data used to develop their model.

Generally, Bea20 best matches the CS17.3 residual patterns when the hypocenters are located near the ends of the faults. In these scenarios, there are clearly defined areas of strong forward and backward directivity effects (Figure 5a). When hypocenters are located closer to the middle of the fault, directivity effects in the residuals tend to be weaker than the Bea20 predictions. Instances of poor match correspond to the absence of apparent directivity effects in the δW_0 (e.g., Figure 4b) or to unexpected azimuthal patterns in the residuals (e.g., Figure 5b).

4.3 Results: Considering Multiple Hypocenters

Continuing with the example from Figure 3, the analysis is repeated for all the 108 hypocenter realizations of this scenario. Using the results from each hypocenter as the dataset, the weighted means and standard deviations of δW_0, f_D, and δW_{0Dir} are calculated at each site. Weights are determined from the Melgar and Hayes (2019) hypocenter location distributions.

Figure 6 maps the means results. For this earthquake, the mean δW_0 has positive valued lobes off the ends of the fault, and regions of negative values between the fault ends; again, broadly consistent with Bea20.

Any given site can experience a range of forward and backward directivity effects, depending on the site location and the hypocenter location. This impacts both the mean and the variability of the δW_0 and f_D taken over hypocenter realizations, and leads to the following observations:

- The mean δW_0 have lower peak amplitudes than those from any given hypocenter realization (the color scale is from -0.5 to 0.5 in Figure 6, as opposed to -1.0 to 1.0 in previous figures showing individual hypocenter realizations). The peak amplitudes of mean δW_0 are lower than the mean f_D in Figure 6.
- The variance δW_0 is larger than the variance of f_D.

Both of these observations generally hold for the larger set of scenarios evaluated, not just the example in Figure 6. These observations indicate that the Bea20 median adjustment may be too large and the model variability may be low.

Even considering these factors, the improvement to the CS17.3 residuals can be quantified using variability reductions for a given scenario. To do so, the residuals δW_0 and δW_{0Dir} from all hypocenter realizations are binned by rupture distance, and within each distance bin, the mean and variance of this pool of residuals are calculated. At this stage, the mean of all residuals within each bin is confirmed to be nearly zero, and so the variances are the weighted sum of squares. In each bin, the ϕ_0^2, ϕ_{0Dir}^2 and their difference ($\phi_{Reduction}^2$) are calculated using Eq. 3. Figure 6 (lower right) shows these variances for each distance bin, with an average $\phi_{Reduction}^2$ across distances less than 40 km of about 0.07 in this example. The variance reduction reduces to zero beyond 80 km, where the Bea20 model reduces to zero effect.

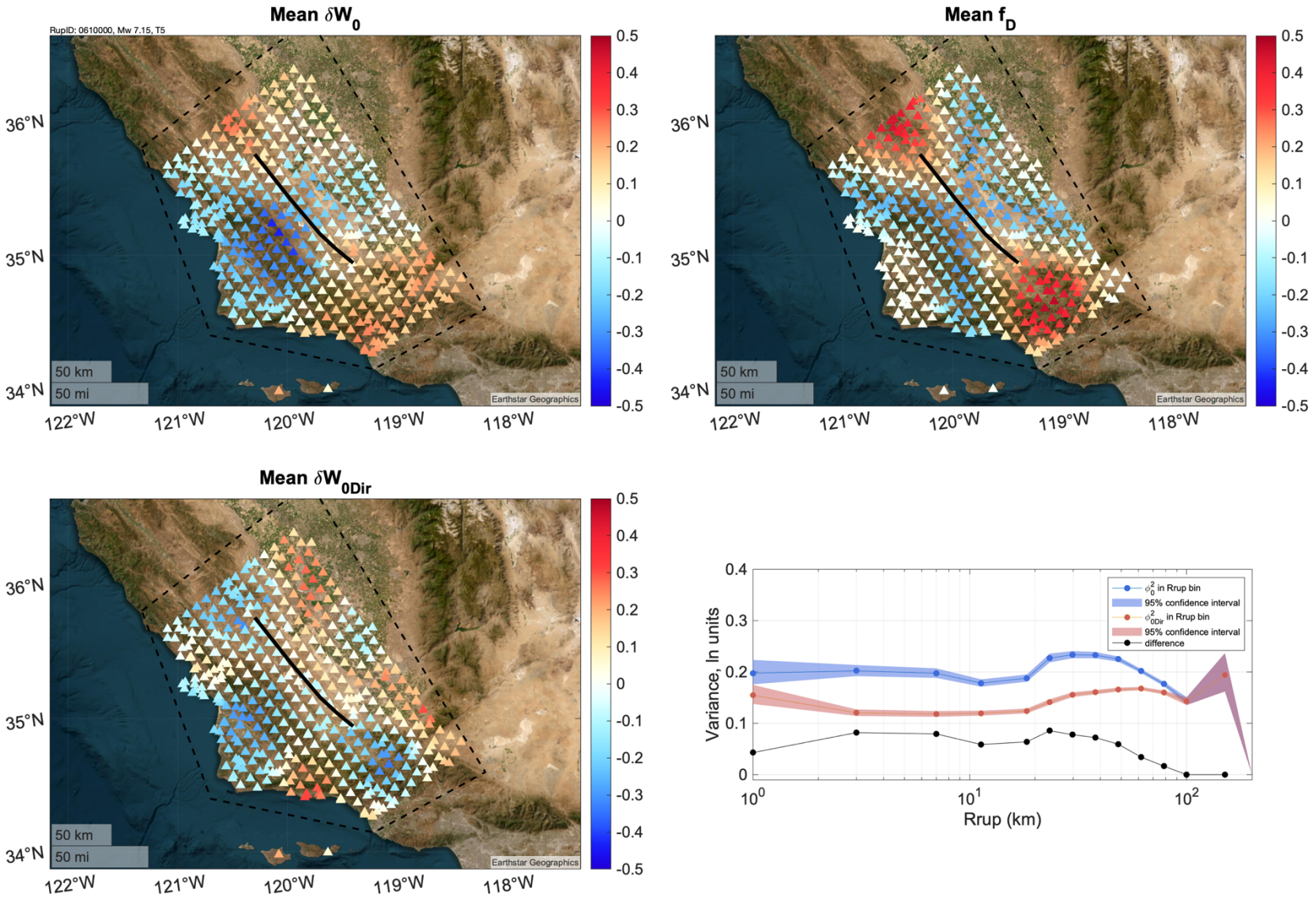

Figure 6. Mean results from 108 hypocenter realization of an example San Andreas scenario earthquake. Maps are of mean δW_0, mean f_D, and mean δW_{0Dir} (T=5 sec). Lower right: ϕ_0^2, ϕ_{0Dir}^2, and $\phi_{Reduction}^2$ binned by rupture distance.

4.4 Results: Aggregate

Section 4.2 described results from individual hypocenter realizations of a given scenario and Section 4.3 described the mean and variance of the results considering the multiple hypocenters of a given scenario. This section aggregates the residuals from the full set of 1034 strike-slip scenarios and all their hypocenter realizations. The residuals from these scenarios are pooled together to estimate the total variance reductions which result from including the Bea20 model, $\phi^2_{Reduction}$ (Eq. 3). To calculate the variances, the residuals from all scenarios are binned by rupture distance. Within each distance bin, the variance is of the residuals from all scenarios and hypocenters.

Figure 7 shows the ϕ_0^2, ϕ_{0Dir}^2 and their difference ($\phi^2_{Reduction}$) calculated from the 1034 strike-slip earthquake scenarios, for the 1D simulations, at T=5 sec. The $\phi^2_{Reduction}$ is between 0.05 and 0.09 for distances less than about 30 km, and then decreases to zero at 80 km distance and greater. Without binning the stations by distance, the T=5 sec $\phi^2_{Reduction}$ for all sites and scenarios is 0.024. This includes hundreds of thousands of stations without a directivity adjustment because their rupture distance is large, and hence no modification to δW_0. Therefore, the distance-dependent $\phi^2_{Reduction}$ is more appropriate for forward application.

Mea23 variances are shown in Figure 8. In the current study, the notation ϕ_0^2 is analogous to the sum of the Mea23 ϕ_0^2 and τ^2_{L2L} components in Figure 8. This is because Mea23 partitioned the between-event residual into systematic source location effects and remaining aleatory event residual. The systematic source location residual was not available in the current study. The sum of Mea23 ϕ_0^2 and τ^2_{L2L} is 0.24 and 0.30 (T=5 sec) for CS17.3 3D and 1D studies, respectively. This is compatible with the ϕ_0^2 from the 1034 scenarios evaluated in this study, shown in Figure 7.

The variance reductions in Figure 7 are significant. Using example values of ϕ_0^2 = 0.30 and $\phi^2_{Reduction}$ = 0.07, the corresponding standard deviations are ϕ_0 = 0.548 and ϕ_{0Dir} = 0.480, where ϕ_0 and ϕ_{0Dir} represent the within-event, within-path, within-site aleatory variability with and without considering rupture directivity. This example represents a 12% reduction in the ϕ component of the aleatory variability, which is large enough to be impactful in PSHA.

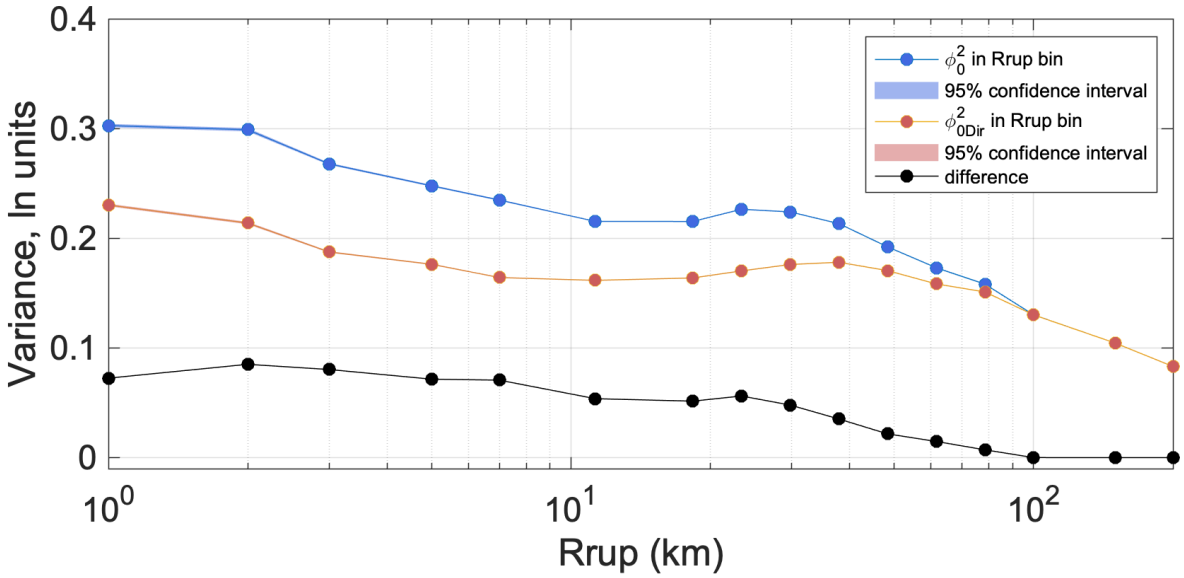

Figure 7. Aggregate ϕ_0^2, ϕ_{0Dir}^2, and $\phi^2_{Reduction}$ at T=5 sec, from 1034 strike-slip 1D simulations, binned by rupture distance.

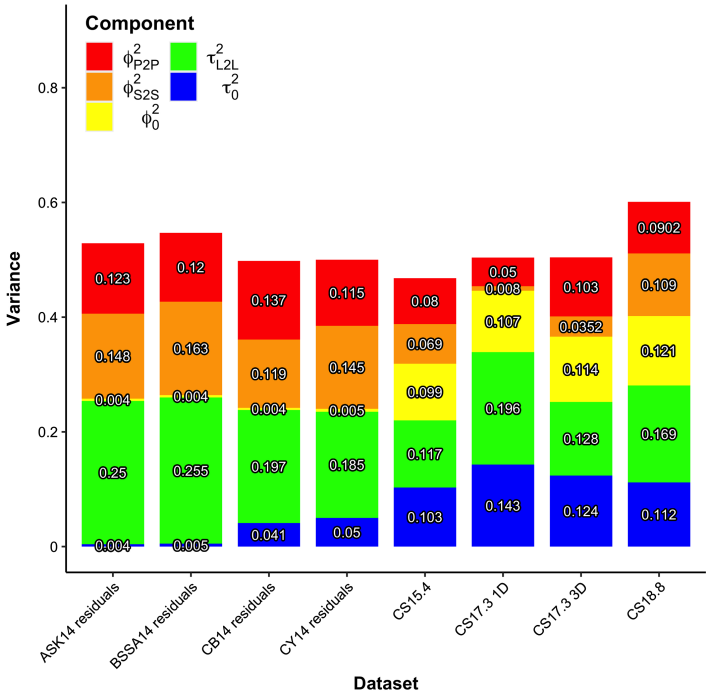

Figure 8. From Meng et al. (2023); variance decomposition from various CyberShake studies, at T=5 sec. Numbers at the center of each component denote variance values. In the current study, the ϕ_0^2 (e.g. Figure 7) is analogous to the sum of the Meng et al. (2023) ϕ_0^2 and τ_{L2L}^2 components, because the systematic source location effects are not partitioned in the current study.

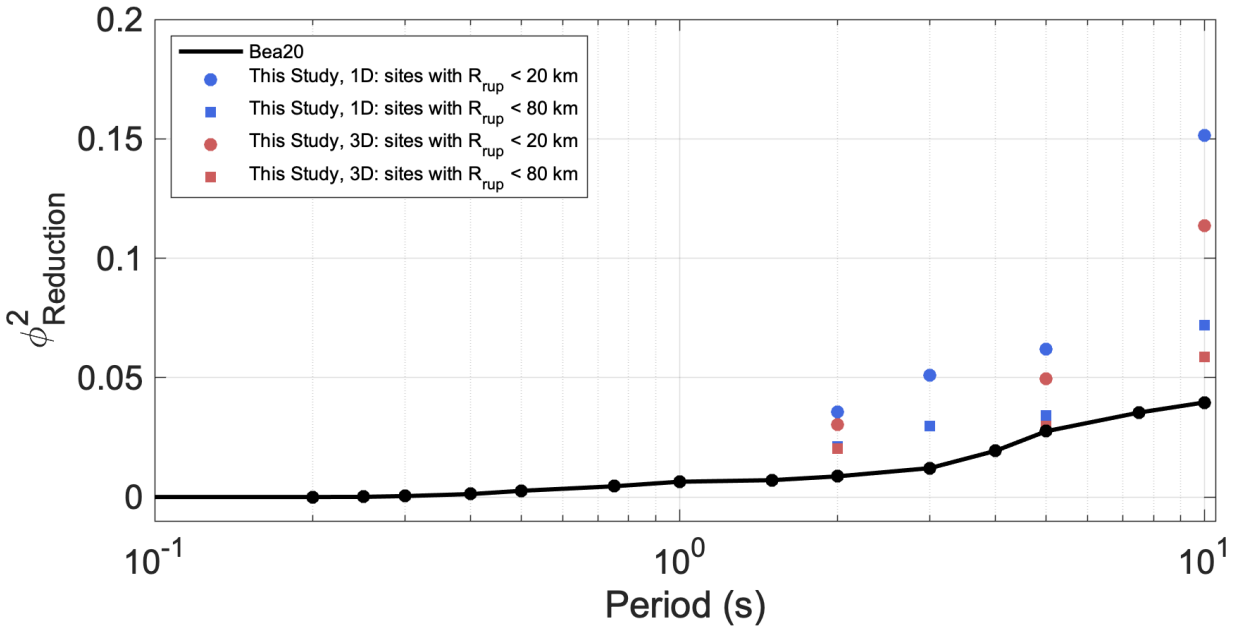

Figure 9. $\phi^2_{Reduction}$ from Bea20 (black) and from this study (blue, red).

The Bea20 model for $\phi^2_{Reduction}$ is shown in Figure 9. The Bea20 reduction was determined empirically from recordings of 22 NGA-West2 earthquakes, using sites within 80 km rupture distance. Bea20 calculated this reduction from a residual analysis similar to those performed here, and for periods between 0.01 and 10 sec. There was not sufficient data in Bea20 to determine distance dependence of the variability reduction.

Figure 9 shows $\phi^2_{Reduction}$ from this study at periods 2, 3, 5, and 10 sec, for the 1D simulations (blue) and 3D simulations (red). The 3 sec period residuals for 3D simulations were not available and so this period was skipped for 3D. Circles are the $\phi^2_{Reduction}$ calculated from all sites with rupture distance less than 20 km, and squares are those calculated from all sites with rupture distance less than 80 km.

5. Summary, Conclusions, and Future Steps

In this study, CS17.3 1D and 3D simulation residuals (δW_0) are used to evaluate the Bea20 directivity model (f_D). The overall performance of Bea20 as compared with the CS17.3 δW_0 is promising, but wide-ranging. There are many instances of source and hypocenter location with residuals patterns and amplitudes matching Bea20 quite well; these correspond to improved median predictions and variability reductions. There are also many instances which do not match as well. This is the same observation Bea20 made with respect to the recorded data used to develop their model.

Generally better model performance occurs when the hypocenters are located near the ends of the faults. In these scenarios, the residuals have clearly defined areas of strong forward and backward directivity effects. When hypocenters are located closer to the middle of the fault plane, directivity effects in the residuals tend to be weaker than the Bea20 predictions. Instances of poorer match can correspond to the absence of apparent directivity effects in the δW_0 or to unexpected azimuthal patterns.

Considering the multiple hypocenter realizations of any given scenario earthquake, two observations are made: The peak amplitudes of mean δW_0 are generally lower than the mean f_D, and the variance δW_0 is generally larger than the variance of f_D. These observations indicate that the Bea20 median adjustment may be too large, and the model variability may be low.

Nonetheless, aleatory variance reductions ($\phi^2_{Reduction}$) resulting from incorporation of Bea20 into the residual analysis are significant. At T=5 sec, residual variance reductions are between 0.05 and 0.09 for sites with rupture distances less than about 30 km. This reduction is larger than the empirically derived reduction from Bea20, which is based on a relatively sparse dataset. A $\phi^2_{Reduction}$ value of 0.07 represents about a 12% reduction in the ϕ component of the aleatory variability, which is large enough to be impactful in PSHA. The next topic to address is the total aleatory variability adjustment that is appropriate in PSHA (Eq. 1); this includes the reduction (this study) and the increase due to changes in the median at a given site due to directivity from all sources and hypocenters. The contribution to the aleatory standard deviation due to the randomized hypocenters for future earthquakes, $\sigma_{i|RH}$, can vary by location. These two components will be combined to provide comprehensive recommendations for treatment of the aleatory variability with Bea20 in PSHA.

Another future topic to address is the distance tapers in Bea20, which were based on observation and were not well constrained. The apparent directivity effects in the CS17.3 simulations extend to much further distances; however, this is also the typical distance range for Moho bounce signals (seismic waves reflected at the Moho boundary; Mori and Helmberger, 1996), and Mea23 identified that these effects appear stronger in the 1D simulations where the seismic-velocity

contrasts are strongest. At this stage, the Bea20 distance tapers are retained because it is the near-fault rupture directivity effects which are of most interest for seismic hazard applications.

6. References

Aagaard, B., J.F. Hall, and T.H. Heaton (2004). Effects of Fault Dip and Slip Rake Angles on Near-Source Ground Motions: Why Rupture Directivity was Minimal in the 1999 Chi-Chi, Taiwan Earthquake, Bull. Seismol. Soc. Am., 94: 155-170.

Abrahamson, N. A. (2000). Effects of rupture directivity on probabilistic seismic hazard analysis, Proceedings from the 6th International Conference on Seismic Zonation, Palm Springs, California.

Bayless, J., and Somerville, P., (2013). Bayless-Somerville Directivity Model, Chapter 3 of PEER Report No. 2013/09, P. Spudich (Editor), Pacific Earthquake Engineering Research Center, Berkeley, CA.

Bayless, J., Somerville, P., Skarlatoudis A. (2020). A Rupture Directivity Adjustment Model Applicable to the NGA-West2 Ground Motion Models and Complex Fault Geometries. Final report. USGS Award No. G18AP00092.

Bozorgnia, Y, NA Abrahamson, L Al Atik, TD Ancheta, GM Atkinson, JW Baker, A Baltay, DM Boore, KW Campbell, BS-J Chiou, R Darragh, S Day, J Donahue, RW Graves, N Gregor, T Hanks, IM Idriss, R Kamai, T Kishida, A Kottke, SA Mahin, S Rezaeian, B Rowshandel, E Seyhan, S Shahi, T Shantz, W Silva, P Spudich, JP Stewart, J Watson-Lamprey, K Wooddell, and R Youngs, 2014. NGA-West 2 research project*, Earthquake Spectra*, **30**, 973-987.

Bray, J. D. and A. Rodriguez-Marek (2004). Characterization of forward-directivity ground motions in the near-fault region. Soil Dynamics and Earthquake Engineering 24(11), 815–828.

Chen, Y., and Baker, J. W. (2019). “Spatial correlations in CyberShake physics-based ground motion simulations.” Bulletin of the Seismological Society of America, (in press).

Donahue, J.L, JP Stewart, N Gregor, Y Bozorgnia (2019) Ground-Motion Directivity Modeling for Seismic Hazard Applications. PEER Report 2019/03

Field, E. H., T. E. Dawson, K. R. Felzer, A. D. Frankel, V. Gupta, T. H. Jordan, T. Parsons, M. D. Petersen, R. S. Stein, R. J. Weldon, et al. (2009). Uniform California Earthquake Rupture Forecast, Version 2 (UCERF 2), Bull. Seismol. Soc. Am. 99, no. 4, 2053–2107

Goulet, CA, NA Abrahamson, PG Somerville, and KE Wooddell, 2015. The SCEC Broadband Platform validation exercise: Methodology for code validation in the context of seismic hazard analyses, Seismol. Res. Lett. 86, 17-26.

Graves, R., Jordan, T. H., Callaghan, S., Deelman, E., Field, E. H., Juve, G., Kesselman, C., Maechling, P., Mehta, G., Okaya, D., Small, P., Vahi, K. (2011), CyberShake: A Physics-Based Seismic Hazard Model for Southern California, *Pure and Applied Geophysics*, 168(3-4), 367–381.

Graves, R and Pitarka, A (2014). Refinements to the Graves and Pitarka (2010) Broadband Ground-Motion Simulation Method. Seismological Research Letters 2014; 86 (1): 75–80. Doi: https://doi.org/10.1785/0220140101

Graves, R and Pitarka, A (2016). Kinematic Ground-Motion Simulations on Rough Faults Including Effects of 3D Stochastic Velocity Perturbations. Bulletin of the Seismological Society of America 2016; 106 (5): 2136–2153. Doi: https://doi.org/10.1785/0120160088

Meng, X., C. Goulet, K. Milner, R. Graves, and S. Callaghan (2023). Comparison of Nonergodic Ground-Motion Components from CyberShake and NGA-West2 Datasets in California, Bull. Seismol. Soc. Am. XX, 1–24, doi: 10.1785/0120220049

Melgar D, and Hayes G (2019). The Correlation Lengths and Hypocentral Positions of Great Earthquakes. Bulletin of the Seismological Society of America. 109(6):2582-2593

Mori, J., and D. Helmberger (1996). Large-amplitude Moho reflections (SmS) from Landers aftershocks, southern California, Bull. Seismol. Soc. Am. 86, no. 6, 1845–1852.

Rodriguez-Marek, A., and Cofer, W. (2009) Incorporation to Forward-Directivity into Seismic Hazard Analysis. Report prepared for Transportation Northwest. Report No. TNW2009-02, Research Agreement No. 430846

Shahi, S. K., (2013). A Probabilistic Framework to Include the Effects of Near-Fault Directivity in Seismic Hazard Assessment, Ph.D. Thesis, Stanford University, Stanford, CA, 226 pp.

Shahi, S. K., and Baker, J. W., (2013). Shahi-Baker Directivity Model, Chapter 4 of PEER Report No. 2013/09, P. Spudich (Editor), Pacific Earthquake Engineering Research Center, Berkeley, CA.

Somerville, P.G., N. Smith, R. Graves and N. Abrahamson (1997). Modification of empirical strong ground motion attenuation relations for the amplitude and duration effects of rupture directivity. Seismol. Res. Lett. 68, 199-222

Spagnulo, E., Herrero, A., and Cultrera, G. (2012). The effect of directivity in a PSHA framework. Geophysical Journal International 191, 616-626.

Spudich, P., Bayless, J. R., Baker, J. W., Chiou, B. S.-J., Rowshandel, B., Shahi, S. K., and Somerville, P. G., (2013). Final Report of the NGA-West2 Directivity Working Group, Pacific Earthquake Engineering Research Center Report PEER-2013/09, Berkeley, CA, 130 pp.

Tarbali, K., Bradley, B., and Baker, J. W. (2016). Seismic hazard analysis and ground motion selection considering directivity effects. Poster presentation at the 2016 QuakeCore Annual Meeting.

Tothong, P., Cornell, C.A., Baker, J.W., (2007), Explicit Directivity-Pulse Inclusion in Probabilistic Seismic Hazard Analysis, Earthquake Spectra, Volume 23, No. 4, pages 867-891, Earthquake Engineering Research Institute.

Villani, M., and N. A. Abrahamson (2015). Repeatable site and path effects on the ground-motion sigma based on empirical data from southern California and simulated waveforms from the CyberShake platform, Bull. Seismol. Soc. Am. 105, no. 5, 2681–2695.

Wang, F., and T. H. Jordan (2014). Comparison of probabilistic seismic-hazard models using averaging-based factorization, Bull. Seismol. Soc. Am. 104, no. 3, 1230–1257.

Watson-Lamprey J.A. (2018). Capturing directivity effects in the mean and aleatory variability of the NGA-West 2 ground motion prediction equations, PEER Report No. 2018/04, Pacific Earthquake Engineering Research Center, University of California, Berkeley, CA.